

Study of Superdeformation in Non-rotating States using the Skyrme-Hartree-Fock Method

Satoshi Takahara*, Naoki Tajima and Naoki Onishi
*Institute of Physics, Graduate School of Arts and Sciences,
University of Tokyo, Komaba, 153-8902, Japan*

Abstract

The superdeformation (SD) in non-rotating states is studied with the HF+BCS method using the Skyrme interaction. In applying the BCS theory, the seniority pairing force is employed, of which strengths are determined in order to reproduce the empirical pairing gap formula, $\bar{\Delta} = 12A^{-1/2}$, through a smooth level density obtained in the Thomas-Fermi approximation. Properties of superdeformation are investigated by calculating potential energy surfaces (PES) for various sets of the pairing force strengths and the Skyrme force parameter for ^{194}Hg and $^{236,238}\text{U}$. The best results are obtained using both the SkM* force and the pairing force strength determined in this paper. By making use of this set of forces, a systematic calculation of SD states is carried out extensively for even-even nuclei for $20 \leq Z \leq 82$. From our calculation, the barriers preventing the decay into the normally deformed states are about twice as high as those predicted by Krieger et al. who used the same Skyrme interaction but a pairing force stronger than ours. The differences of the present results from the Nilsson-Strutinsky calculation are analyzed.

PACS: 21.10.Ky; 21.10.Pc; 21.10.Tg; 21.60.Jz

Keywords: Zero-spin superdeformation; Skyrme-Hartree-Fock;

1 Introduction

In the last decade, superdeformed (SD) bands have been studied extensively both experimentally and theoretically. Since the first observation of SD bands was made in ^{152}Dy nucleus in 1986[1], they have been found in four mass regions, i.e., $A \sim 80$ [2], 130, 150 and 190[3, 4, 5]. The theoretical studies of SD have helped to clarify understanding of nuclear deformation. Indeed the present authors carried out an extensive investigation of normal deformations using Skyrme-Hartree-Fock method and reproduced the deformation for almost all even-even nuclei[6]. Therefore we thought it would be worthwhile to use the method to calculate SD.

*Corresponding author. E-mail staka@hep1.c.u-tokyo.ac.jp

These SD bands have been found only at high spins so far, mainly because of the experimental method of formation of SD bands. It is expected that they may be present at zero spin, like fission isomers in actinide nuclei. It may require elaborate calculations to search for SD states in the two-dimensional space of angular momentum and quadrupole moment. Therefore, as a first step, we tried to study SD in non-rotating states and did not crank the mean field.

In this paper, we looked for SD in non-rotating states using numerical calculations of potential energy surfaces (PES) employing the Hartree-Fock(HF) with the Skyrme interaction together with the BCS method using the seniority force. A characteristic feature of our calculations is that the single-particle wave functions are expressed in a three-dimensional Cartesian-mesh representation as described in Ref. [7]. This representation enables one to obtain wave functions for various shapes in a single framework, without any prejudice about shape, i.e., one need not optimize the deformation of the basis (like the three oscillator frequencies ω_κ of the anisotropic harmonic-oscillator basis) for each solution. Solving the mean-field equations in this representation requires, however, a large amount of computation which can be accomplished only with supercomputers.

In this paper we utilize an HF+BCS code *EV8*[7], in which the mean-field potential is assumed to be symmetric for reflections in the xy -, yz -, and zx -planes (the point group D_{2h}). We set the mesh size to 1 fm, while the size of the box is $15 \times 15 \times 16$ fm. We put an octant of a nucleus at a corner of the box. For the BCS part, we employ the seniority force.

In sect. 2, we compare various parameter sets of the Skyrme force to see how accurately they can reproduce the excitation energy of the SD band head of ^{194}Hg . We explain our method to determine the pairing force strengths. We also show how strongly the pairing correlation affects the properties of SD states. In sect. 3, we study the fission isomers in $^{236,238}\text{U}$. In sect. 4, we systematically search large-deformation solutions employing the SkM* force. We compare the results with those obtained by Krieger et al. [8], who used the same Skyrme force but stronger pairing force strengths. In sect. 5, we also analyse the results obtained with the Nilsson-Strutinsky method. Section 6 is a summary of the present paper.

2 Superdeformation in ^{194}Hg

Recently, Khoo et al. [9] determined the excitation energies and the spins of a SD band in ^{194}Hg down to $I^\pi = 8^+$. By extrapolating the spectrum to $I = 0$, they could predict reliably the excitation energy of the band head to be 6.017 MeV.

In Table 1, theoretical predictions (listed in Ref. [9]) are shown to be compared with the extrapolated value. One can see that all of the predictions are either lower or higher than the extrapolated value by at least 0.9 MeV.

Fig. 1 presents the results of our HF+BCS calculations using nine sets of the Skyrme force parameters. We draw PES curves as functions of the quadrupole deformation parameter δ defined as

$$\delta \equiv \frac{3\langle \hat{Q}_z \rangle}{4\langle \hat{r}^2 \rangle}, \quad (1)$$

where \hat{Q}_z is the axially symmetric mass quadrupole moment, $\hat{Q}_z \equiv 2\hat{z}^2 - \hat{x}^2 - \hat{y}^2$, and \hat{r}^2 is the squared mass radius, $\hat{r}^2 \equiv \hat{x}^2 + \hat{y}^2 + \hat{z}^2$. The excitation energy E^* of the SD minimum at $\delta \sim 0.5$ measured from the ground-state minimum at $\delta \sim -0.1$ is given in parentheses in units of MeV for each force.

The left-hand portion of Fig. 1 shows the results with five widely-used Skyrme interactions; SIII[14], SkSC4[15], SkM*[16], SkP[17], and SGII[18]. One can see that the SkM* as well as the SkP forces are the best ones to reproduce the experimental value of E^* . On the other hand, the SIII and the SkSC4 forces make the nucleus too stiff against deformation, while the SGII too soft. From a macroscopic point of view, the softness toward deformation is determined by the smallness of the surface energy coefficient a_s [16] specific to each force. The SkM* is a force adjusted so as to reproduce the fission barrier height of ^{240}Pu and thus is expected to have the correct surface energy coefficient.

The right-hand portion of Fig. 1 gives the results for four new parameter sets, SkI2 - SkI5[19]. These forces have different features involving the density dependence of the spin-orbit potential. The standard Skyrme interactions, such as SkI2 and SkI5, produce spin-orbit potentials for neutrons which are proportional to the gradient of $\rho + \rho_n$, where ρ (ρ_n) denotes the nucleon (neutron) density. On the other hand, the spin-orbit potentials produced by SkI3 and SkI4 are proportional to the gradient of ρ and roughly $\rho - \rho_n (= \rho_p)$, respectively. The parameters of SkI2 - SkI4 were determined by fitting to the same set of nuclear properties. A slightly different set of the quantities was adjusted to determine SkI5. Among these four forces, SkI3 reproduces the experimental value of E^* very accurately. On the other hand, SkI2 and SkI5 (i.e., standard Skyrme forces) make the nucleus too soft against deformations while SkI4 too stiff. This fact is consistent with the relativistic mean-field theory, whose “spin-orbit potential” has a similar density dependence[19] to that of SkI3.

We now discuss the effects of pairing. Using the same Skyrme interaction SkM*, Krieger’s calculation[8] and ours give different results, which originate in the difference of the strengths of the seniority interaction used to describe the pairing correlation.

Krieger et al. used the pairing force strengths G_τ ($\tau=n$ for neutrons and $\tau=p$ for protons) given by the following formula,

$$G_p = \frac{17.5}{11 + Z}, \quad G_n = \frac{16.5}{11 + N}, \quad [\text{MeV}]. \quad (2)$$

On the other hand, we determined the strengths G_τ such that the so-called classical empirical formula of the average pairing gap,

$$\bar{\Delta}_\tau = \frac{12}{\sqrt{A}} \quad [\text{MeV}], \quad (3)$$

is reproduced for shell-effect-averaged level density obtained in the Thomas-Fermi approximation. The pairing-active space is the same in both the Krieger et al. treatment and ours: single-particle levels below “the Fermi level plus 5 MeV” were taken into account in the BCS calculation in both cases. See Ref. [6] for details of our calculations.

The effects of the change in the pairing strengths are demonstrated in Fig. 2. The top portion shows the pairing gap of protons. The Krieger et al. strength ($G_p=0.192$ MeV) gives a rather large pairing gap ($\Delta_p < 1.8$ MeV), while our pairing strength ($0.145 <$

$G_p < 0.168$ (MeV)) produces a reasonable size gap ($\Delta_p < 1.2$ MeV) for $0.2 < \delta < 0.6$. On the other hand, the pairing gap of neutrons does not differ very much between the two calculations and has a reasonable size as shown in the middle portion of Fig. 2. This is a direct consequence of the fact that the Krieger et al. strength ($G_n = 0.132$ MeV) and our strength ($0.114 < G_n < 0.126$ (MeV)) do not differ very much.

The PES curves are shown in the bottom portion of Fig. 2. One can see that the reduction of the proton's pairing force strength raises the energy by 3 MeV at the barrier and by 1 MeV at the SD minimum while leaving the energy almost unchanged at the oblate minimum. Consequently, Krieger et al. obtained $E^* = 5.0$ MeV, which is lower than our value by 1.3 MeV, and the barrier height (defined in the figure) $E_B = 1.8$ MeV, which is lower than our value by 1.7 MeV.

Note that the half-life of the SD band head due to decay into the normal-deformation (ND) well is longer for higher barriers. We have estimated the half-life using WKB approximation ($f_B = 10$ in Eq. (9)). The resulting half-life is 6×10^{-17} sec for the Krieger et al. pairing force strengths while it is 1×10^{-13} sec for our strengths. The difference amounts to a factor of about 10^3 .

In Fig. 3, we show the Nilsson diagram obtained by self-consistent mean-field calculation for ^{194}Hg using SkM*. In the case of proton, one can see clearly a lacuna at $Z = 80$ in the vicinity of $\delta \sim 0.52$. On the other hand, there is no clear lacuna for $N = 114$ in the case of neutron. But the level density near the Fermi surface is relatively small so that neighboring isotopes have an SD. This is consistent with the fact that the proton pairing gap sharply decreases, while the neutron pairing gap does rather smoothly at $\delta \sim 0.52$, as we showed in Fig. 2.

The analysis of the SD state in ^{194}Hg indicates the appropriateness of our pairing force strengths combined with the SkM*, SkP, and SkI3 forces for the HF potential.

3 Fission Isomers

We have also applied the HF+BCS method to fission isomers. Among several tens of actinide nuclei having fission isomers, ^{236}U and ^{238}U are the only ones whose fission isomers were observed to decay electromagnetically into ND states[20]. The energy of the gamma-ray tells us the excitation energy of the fission isomer, while the measured half-life gives information on the barrier between the SD and the ND wells.

We estimate the half-lives as

$$\tau_{1/2} = \frac{\ln 2}{nP}, \quad (4)$$

where the half-life $\tau_{1/2}$ is inversely proportional to two quantities. One is the quantity, n , the number of assaults in the SD well, which may be estimated as

$$n = \frac{\omega_{\beta\text{-vib}}}{2\pi}, \quad (5)$$

where $\omega_{\beta\text{-vib}}$ is the angular frequency of the β -vibration in the SD well. We assume that $\omega_{\beta\text{-vib}}$ scales as $A^{-1/6}$ and that $\hbar\omega_{\beta\text{-vib}} = 1$ MeV for $A = 150$. The other quantity, P , is

the penetration probability through the barrier into the ND well, which is related to the action S in the WKB approximation as

$$P = \exp(-S), \quad (6)$$

$$S = \frac{2}{\hbar} \int_{\beta_1}^{\beta_2} \sqrt{2B(\beta)(V(\beta) - E)} d\beta. \quad (7)$$

On the right hand side of Eq. (7), β_2 is the deformation of the SD isomer while β_1 is the deformation in the ND well where the total energy is the same as that of the SD isomer, i.e., $V(\beta_1) = V(\beta_2) = E$. We relate β to δ defined by Eq. (1) as $\beta = (16\pi/45)^{1/2}\delta \simeq 1.06\delta$. The action S takes on large values when the barrier is large and broad and/or when the collective mass $B(\beta)$ is large.

The collective mass for small-amplitude irrotational hydro-dynamical motions is expressed as[21]

$$B_\lambda = \frac{\rho R_0^5}{\lambda} = \frac{3Am_N R_0^2}{4\lambda\pi}, \quad (8)$$

where $\lambda(= 2)$ is the multipolarity of the motion, ρ the nucleon density inside the nucleus ($= 3Am_N/4\pi R_0^3$), R_0 the nuclear radius ($= 1.2A^{1/3}$ fm), A the mass number, and m_N the bare nucleon mass. We express the collective mass in units of B_2 , neglecting the dependence on deformation:

$$B(\beta) = B_2 f_B. \quad (9)$$

The empirical enhancement factor f_B varies between 10 and 40 when it reproduces the quadrupole vibrational levels of spherical nuclei[22].

Table 2 gives the experimental and theoretical values of the excitation energies and the partial half-lives of the fission isomers. The first line gives the experimental values, while the second line shows the results calculated by Chinn et al. [23]. They employed the Hartree-Fock-Bogoliubov (HFB) method with the Gogny D1 force[24]. They calculated the half-lives by reducing the Hill-Wheeler equation for the generator coordinate method (GCM) to a Schrödinger equation with the Gaussian overlap approximation. The fifth and the sixth lines give the results obtained by Krieger et al. [26], who employed the HF+BCS method with the SkM* force and the pairing force strengths fitted so as to reproduce the experimental pairing gaps. They estimated the half-lives with the GCM without further approximations. Lines 7-10 are the results of our calculations using the SkM* force. We determine the pairing force strengths in the same manner as we did for ^{194}Hg .

Chinn et al. reproduced the excitation energy of ^{238}U rather well (the error is +11%). In Ref. [25], Krieger et al. obtained a better agreement with the experimental value (the error is -11%) by taking into account the correlations in both the ground and SD states with the GCM method than without the correlation (the error is +17%). Recently, they revised the calculations [26] with slightly weaker pairing strengths so as to reproduce the experimental pairing gaps ($G_n = 0.1067 \rightarrow 0.0955$ [MeV], $G_p = 0.1621 \rightarrow 0.1505$ [MeV]). As a result, they obtained improved results. For ^{238}U , the error is +6% for HF+BCS, +2% with GCM. For ^{236}U , the error is +5% for HF+BCS, +1% with GCM. This also shows that the excitation energy of the very deformed isomers is very sensitive to the strengths of pairing force.

Figs. 4 and 5 show the PES curves of $^{236,238}\text{U}$, respectively, which we have calculated employing the SkM*, SIII, and SkP forces. The excitation energies for ^{236}U and ^{238}U are overestimated by 1.8 MeV and 0.7 MeV, respectively, with the SkM* force. Using SIII or SkP makes the agreement worse.

The partial half-lives were not reproduced very accurately either by Chinn et al. [23] or Krieger et al. [26]. As for our calculations, we have to determine the enhancement factor f_B before estimating the half-lives. Conversely, when the factor f_B is adjusted to reproduce the experimental half-lives, the resulting values are $f_B = 13.7$ for ^{236}U and $f_B = 10.4$ for ^{238}U .

Our calculations of the half-lives are crude because of our use of the WKB approximation. There are many factors which can strongly influence the calculation of the half-lives. Our calculation takes into account the landscape of the potential energy curve and the collective mass. It does not take into account the triaxial deformation, the level density in the ND well and the angular momentum projection effect.

4 Systematics of the non-rotating SD

From the analysis in the last two sections, SkM* seems the best Skyrme force to describe non-rotating SD states. With this force, we have explored a wide area of the nuclear chart ranging from $Z = 20$ to $Z = 82$ for the SD states at zero spin in even-even nuclei. To compare the energy of zero spin states with experiments, one should perform the angular momentum projection. In this paper, we approximate the zero-spin states by non-rotating states.

An earlier microscopic attempt to explore SD at zero spin was made by Bonche et al. [27] for the Os-Pt-Hg region using the HF+BCS with the SIII force. Later, Krieger et al. [8] changed the force to SkM* and performed an extensive calculation covering from $^{62}\text{Sm}_{126}$ to $^{92}\text{U}_{146}$ to obtain SD minima for 148 nuclei.

We employed the same Skyrme force as Krieger et al. used. However, the results of our calculations are significantly different as we will show at the end of this section. The difference originates in their proton pairing-force strength, which seems too strong as demonstrated clearly in sect. 2 for ^{194}Hg .

Our calculations do not cover very neutron-rich nuclei, unlike the calculations by Krieger et al., because the pairing correlation among neutrons cannot be correctly described within the HF+BCS scheme for these nuclei. When the Fermi level approaches zero from below, the continuum single-particle states are involved strongly in the pairing correlation. This coupling cannot be treated in the HF+BCS scheme, which relies on an assumption that the pair-scattering matrix elements are independent of the single-particle wave functions (e.g., constant as in the seniority force). For the correct description of the coupling, one has to switch from the HF+BCS to the HFB scheme[17].

In order to search for the SD solutions, we took the following steps:

i) We prepared an initial wave function by either using the solution for a neighboring nucleus or taking the eigenstate of the Nilsson potential of appropriate deformation.

ii) If the quadrupole deformation parameter δ of the initial wave function was smaller than 0.6, we exerted an external potential proportional to \hat{Q}_z on the initial wave function

until δ exceeded 0.6. Then, we switched off the external potential.

iii) We let the wave function evolve in imaginary time [28] by itself. If it converged to a local minimum with $\delta > 0.35$, we regarded that the nucleus has an SD isomeric state. If δ became less than 0.35 in the course of the self evolution, we concluded that the nucleus does not have an SD state.

iv) If the nucleus had an SD minimum, we calculated the potential energy curve for $0 \leq \delta \leq 0.6$ ($-0.3 \leq \delta \leq 0.6$ for $Z=80$) by imposing a constraint on \hat{Q}_z . We also imposed $\langle x^2 - y^2 \rangle_{\text{mass}} = 0$ for the sake of a fast convergence. This step required more than ten times as long computation time as the previous three steps. It was necessary, however, to calculate the excitation energy and the barrier height, which are necessary to estimate the half-life of the isomer.

Following the above prescription, we explored 642 even-even nuclei with $20 \leq Z \leq 82$ and found SD minima in 118 nuclei. In Table 3, we give the deformation δ , the excitation energy E^* , and the barrier height E_B of the thus-obtained large-deformation (i.e., $\delta > 0.35$) solutions of 118 nuclei.

These results are presented again graphically in Fig. 6. The top portion shows the size of the quadrupole deformation δ in terms of the diameter of the circles.

The middle portion gives the excitation energy measured from the ground state. The diameter of the circles is inversely proportional to the excitation energy. Circles are solid (open) when the excitation energy is less (greater) than 8 MeV: SD states designated by solid circles are easier to observe experimentally than those symbolized by open circles. When the SD state is the ground state, the circle is not drawn.

The bottom portion shows the barrier height between the SD minimum and the ground state in terms of the diameter of circles. The circles are solid (open) when the barrier height is greater (less) than 0.5 MeV: SD states indicated by open circles are unlikely to have long half-lives. When the SD state is the ground state, the circle is not drawn.

The SD states obtained from our calculations can be classified into nine groups.

1. $34 \leq Z \leq 42, 36 \leq N \leq 42$ (12 nuclei)

These nuclei around ${}^{76}_{38}\text{Sr}_{38}$ are superdeformed in the ground state. The axis ratio is about 3:2 ($\delta \sim 0.38$). They have no other prolate minima in the range $0 < \delta < 0.6$.

2. $44 \leq Z \leq 48, 44 \leq N \leq 50$ (10 nuclei)

These nuclei around ${}^{92}_{46}\text{Pd}_{46}$ have the largest deformations ($\delta \geq 0.6$) among the nuclei which we calculated. These SD states are, however, difficult to detect because the excitation energies are rather high (> 10 MeV) while the barrier heights are rather low (< 1 MeV).

3. $58 \leq Z \leq 60, 60 \leq N \leq 66$ (6 nuclei)

These nuclei around ${}^{122}_{58}\text{Ce}_{64}$ have rather large deformations ($\delta \sim 0.35$) in the ground state.

4. $68 \leq Z \leq 82, 80 \leq N \leq 102$ (29 nuclei)

Many nuclei have SD minima in this region near the proton-drip line. The deformations are in the range $0.41 \leq \delta \leq 0.63$. Some of them have low E^* and high E_B . For example, ${}^{172,174,176}\text{Hg}$ have $E^*=5.2, 4.5,$ and 4.1 MeV and $E_B=2.9, 2.0,$ and 1.2 MeV, respectively.

5. $74 \leq Z \leq 82, 106 \leq N \leq 134$ (48 nuclei)

This group corresponds to the $A \sim 190$ region where many high-spin SD rotational bands have been observed experimentally. The deformations are in the range $0.46 \leq \delta \leq 0.55$.

In Fig. 7 we show how the landscape of the PES curve changes along the $Z = 82$ isotope chain, which runs through this and the previous groups. One can see that, approaching to the spherical magic of $N = 126$, the barrier height becomes higher while the excitation energy also increases. Indeed, $^{208}_{82}\text{Pb}_{126}$ has the largest E^* (23 MeV) and E_B (6.5 MeV) in this group. The former effect makes the half-lives of the SD states in $N \sim 126$ nuclei very long according to Eqs. (4)-(7). However, the latter effect makes those states difficult to detect experimentally.

Judging from the location of each nucleus in (E^*, E_B) plane, we think that the most promising nuclei for experimental observations in this group are $^{188,190,192}\text{Hg}$, which have $E^*=3.7, 4.1, \text{ and } 4.9$ MeV and $E_B=1.1, 2.4, \text{ and } 3.6$ MeV, respectively. On the other hand, ^{194}Hg , discussed in sect. 2, is less promising than these three isotopes because it has a higher E^* but a little smaller E_B than ^{192}Hg has.

6. $38 \leq Z \leq 40, 60 \leq N \leq 68$ (8 nuclei)

Nuclei near $^{104}_{40}\text{Zr}_{64}$ have rather large deformations ($\delta \sim 0.35$) in the ground state.

7. $48 \leq Z \leq 50, N = 80$ (2 nuclei)

$^{128}_{48}\text{Cd}_{80}$ and $^{130}_{50}\text{Sn}_{80}$ have SD minima at $\delta \sim 0.56$. The quantum fluctuation of shape is expected to wash out these minima because the excitation energy is very high (> 20 MeV) while the barrier is very low (< 130 keV).

8. $Z = 58, N = 80$ (1 nucleus)

$^{138}_{58}\text{Ce}_{80}$ has a SD minimum at $\delta = 0.44$, which seems too shallow (the barrier height is 120 keV) to confine the collective wave function.

9. $Z = 64, 90 \leq N \leq 92$ (2 nuclei)

$^{154}_{64}\text{Gd}_{90}$ and $^{156}_{64}\text{Gd}_{92}$ have SD minima with very low barriers (~ 80 keV). The PES of a neighboring isotope ^{152}Gd is plotted in Fig. 8, where the SD minimum existing in ^{154}Gd has become a shoulder. The behavior of the pairing gaps shown in the figure suggests that the SD shell gaps occur at somewhat different deformations between protons and neutrons.

These nuclei are in the $A \sim 150$ region where high-spin SD rotational bands have been discovered in many nuclei. However, only two nuclei have the SD minimum at zero spin in contrast to the situation for the $A \sim 190$ region. This is in agreement with the fact that SD rotational bands are found as low as $I = 20(10)\hbar$ in this ($A \sim 190$) mass region.

Incidentally, we have not found any zero-spin SD states in nuclei belonging to the $A \sim 130$ mass region of high-spin SD rotational bands.

In Figs. 9 and 10, we compare E^* and E_B of Krieger et al. with our results. One can see that the excitation energies of the SD states are not very different while our barrier

heights are about twice as high as the values of Krieger et al. This change is brought about by our weaker pairing force strengths.

5 Comparison with the results of the Nilsson-Strutinsky method

The Nilsson-Strutinsky(NS) method is a convenient and well-established method to treat nuclear deformations. Because NS computation is much simpler than self-consistent-field calculations, it seems worth doing another systematic survey of SD isomers using the NS method in order to compare the results with those of the Skyrme-HF method for the same nuclei. Our survey using NS method provides a useful overview of the situation outside the region investigated in the last section.

We have utilized a program for the standard Nilsson-Strutinsky calculation[29] provided by Y. R. Shimizu[30], which takes into account two axially symmetric deformations, i.e., the quadrupole deformation ϵ_2 and the hexadecapole deformation ϵ_4 . For each value of ϵ_2 , the value of ϵ_4 is optimized so as to minimize the total energy.

The standard values given in Table 1 of Ref. [31] are used for the parameters κ_N and μ_N of the Nilsson potential. The pairing correlation is active for single-particle levels within $\pm 1.2\hbar\omega$ from the Fermi level, while the strengths of the pairing force are determined such that the smoothed pairing gap becomes $\bar{\Delta} = 13A^{-1/2}$ MeV. The parameters of the macroscopic part[32] are $a_s = 17.9439$ MeV, $\kappa_s = 1.7826$, and $R_c = 1.2249A^{1/3}$ fm. See Ref. [33] for calculational details.

With this model one can calculate the entire region of the nuclear chart, i.e., from the proton drip line to the neutron drip line: The model does not suffer from the problem of neutron pairing in neutron-rich nuclei explained in sect. 4 because the Nilsson potential does not have a continuum spectrum. Concerning the expected enhancement of the pairing due to the coupling with the continuum states, however, the present model simply neglects its influences.

The calculation for 2000 even-even nuclei can be completed in a few hours with an ordinary personal computer owing to the simpleness of the NS method itself and also to the specialization of the code to non-rotating axially symmetric states.

Fig. 11 displays the resulting deformations ϵ_2 , excitation energies E^* , and barrier heights E_B of the SD minima at $\epsilon_2 > 0.35$. Let us discuss the results according to the grouping employed in sect. 4.

1. $38 \leq Z \leq 40, 36 \leq N \leq 38$

The area of this island of zero-spin SD states is much smaller than in the Skyrme-HF results.

2. $48 \leq Z \leq 50, 44 \leq N \leq 48$

The number of nuclei is reduced from 10 to 4.

3. $58 \leq Z \leq 60, 60 \leq N \leq 66$

None of the 6 nuclei were found to display SD isomers in the NS model.

4. $70 \leq Z \leq 80, 80 \leq N \leq 102$

The number of nuclei is almost unchanged (thirty), but the number of neutron deficient (rich) nuclei is decreased (increased). The appearance of SD around Pb-Hg-Pt isotopes is quite similar in the Skyrme-HF and the NS methods. However, the details are different. For example, the PES of the Skyrme-HF has a smaller E^* and a larger E_B than that of the NS model for the Pb isotopes.

5. $Z + N > \sim 200$

One can see that the group No. 5 found in the Skyrme-HF is a part of a huge area extending to $Z > 82$ and/or $N > 126$. In the actinide region there exist fission isomers for almost all the nuclei except in a rectangle-like area $Z \geq 102$ and $N \leq 186$, where large deformation minima do not exist and the nucleus goes into fission directly from the ground state.

6. $38 \leq Z \leq 40, 60 \leq N \leq 68$

None of 8 nuclei in this region show SD isomers.

7,8. $36 \leq Z \leq 62, 78 \leq N \leq 82$

This region extending vertically includes small islands of Nos. 7 and 8 listed in sect. 4.

9. $Z = 68, 86 \leq N \leq 88$

Compared with the island No. 9 of the Skyrme-HF results, SD isomers are found at Z and N values differing by +4 and -4, respectively.

10. $46 \leq Z \leq 54, 98 \leq N \leq 102$

The nine nuclei above the neutron-drip line have zero-spin SD states. The deformations are in the range $0.63 \leq \delta \leq 0.64$.

11. $54 \leq Z \leq 66, 118 \leq N \leq 130$

Each of twenty-seven nuclei above the neutron-drip line has a large-deformation ($0.36 \leq \delta \leq 0.41$) solution mostly in the ground state.

6 Conclusions

In this paper we studied the super-deformed states at zero spin using the HF+BCS method with the Skyrme interactions.

In sect. 2, we compared nine parameter sets of the Skyrme force in their ability to reproduce the SD bandhead of ^{194}Hg . The best agreements of the excitation energy with the experimental value are obtained for the SkM*, SkP, and SkI3 interactions. The contour of the PES curve, especially the barrier height, is found to be very sensitive to the pairing force strengths.

In sect. 3, we presented our studies of the fission isomers in $^{236,238}\text{U}$. The agreement with experimental excitation energies is better for the SkM* force than for the SkP and SIII forces. The SkM* seems to be the best one among the available parameter sets of the standard Skyrme interaction for the treatment of large deformations.

In sect. 4, we presented our studies of the systematics of large-deformation ($\delta > 0.35$) states of even-even nuclei using the SkM* force. We searched 642 even-even nuclei with $20 \leq Z \leq 82$ and found 118 SD minima. We analyzed the systematics of the deformation, excitation energy, and barrier height of these SD minima.

The difference between our calculation and an earlier systematic study by Krieger et al. using the same Skyrme force lies in the strengths of the pairing force. We determine the strengths such that the empirical formula $\bar{\Delta} = 12A^{-1/2}$ MeV is reproduced for the averaged single-particle level density using the Thomas-Fermi approach. Our strengths determined in this manner are weaker than those adopted by Krieger et al. As a consequence, the barrier heights are doubled while the excitation energies are not changed so much.

In sect. 5, we also used the Nilsson-Strutinsky method to do another systematic comparison with the results of our Skyrme-HF calculation.

The results of our calculations presented in Table 3 are available electronically through the Internet at <http://nt2.c.u-tokyo.ac.jp/hf/sdzs/>.

The authors thank Dr. P. Bonche, Dr. H. Flocard, and Dr. P.-H. Heenen for providing the HF+BCS code *EV8*. They are also grateful to Dr. Y.R. Shimizu for providing the Nilsson-Strutinsky code and commenting on the corresponding part of this paper. We thank Dr. P.-H. Heenen, Dr. M.S. Weiss and Dr. S.J.Krieger for useful discussions. A part of this work was financially supported by RCNP, Osaka University, as RCNP Computational Nuclear Physics Project (No. 95-B-01). The remaining part of the calculations were performed with a super computer VPP500 at RIKEN (Research Institute for Physical and Chemical Research, Japan).

References

- [1] P. J. Twin, B. M. Nyako, A. H. Nelson, J. Simpson, M. A. Bentley, H. W. Cranmer-Gordon, P. D. Forsyth, D. Howe, A. R. Mokhtar, J. D. Morrison, J. F. Sharpey-Schafer, G. Sletten, *Phys. Rev. Lett.* **57** (1986) 811.
- [2] C. Baktash, D. M. Cullen, J. D. Garrett, C. J. Gross, N. R. Johnson, W. Nazarewicz, D. G. Sarantites, J. Simpson, T. R. Werner, *Phys. Rev. Lett.* **74** (1995) 1946.
- [3] P. J. Nolan and P. J. Twin, *Annu. Rev. Nucl. Part. Sci.* **38** (1988) 533.
- [4] S. Åberg, *Nucl. Phys.* **A520** (1990) 35c.
- [5] R. V. F. Janssens and T. L. Khoo, *Annu. Rev. Nucl. Part. Sci.* **41** (1991) 321.
- [6] N. Tajima, S. Takahara and N. Onishi, *Nucl. Phys.* **A603** (1996) 23.
- [7] P. Bonche, H. Flocard, P.-H. Heenen, S.J. Krieger and M.S. Weiss, *Nucl. Phys.* **A443** (1985) 39.
- [8] S. J. Krieger, P. Bonche, M. S. Weiss, J. Meyer, H. Flocard, P.-H. Heenen, *Nucl. Phys.* **A542** (1992) 43.
- [9] T. L. Khoo, M. P. Carpenter, T. Lauritsen, D. Ackermann, I. Ahmad, D. J. Blumenthal, S. M. Fischer, R. V. F. Janssens, D. Nisius, E. F. Moore, A. Lopez-Martens, T. Dossing, R. Kruecken, S. J. Asztalos, J. A. Becker, L. Bernstein, R. M. Clark, M. A.

- Deleplanque, R. M. Diamond, P. Fallon, L. P. Farris, F. Hannachi, E. A. Henry, A. Korichi, I. Y. Lee, A. O. Macchiavelli, F. S. Stephens, Phys. Rev. Lett. **76** (1996) 1583.
- [10] W. Satula, S. Cwiok, W. Nazarewicz, R. Wyss, A. Johnson, Nucl. Phys. **A529** (1991) 289.
- [11] R. Chasman, Phys. Lett. **B219** (1989) 227.
- [12] J. P. Delaroche, M. Girod, J. Libert, I. Deloncle, Phys. Lett. **B232** (1989) 145.
- [13] M. A. Riley, D. M. Cullen, W. Nazarewicz, A. Alderson, I. Ali, P. Fallon, P. D. Forsyth, F. Hanna, S. M. Mullins, J. W. Roberts, J. F. Sharpey-Schafer, P. J. Twin, R. J. Poynter, R. Wadsworth, M. A. Bentley, A. M. Bruce, J. Simpson, G. Sletten, T. Bengtsson, R. Wyss, Nucl. Phys. **A512** (1990) 178.
- [14] M. Beiner, H. Flocard, Nguyen van Giai and P. Quentin, Nucl.Phys. **A238** (1975) 29.
- [15] Y. Aboussir, J.M. Pearson, A.K. Dutta and F. Tondeur, Nucl. Phys. **A549** (1992) 155; Atomic Data Nucl. Data Tables **61** (1995) 127.
- [16] J. Bartel, P. Quentin, M. Brack, C. Guet and H.-B. Hakansson, Nucl.Phys. **A386** (1982) 79.
- [17] J. Dobaczewski, H. Flocard and J. Treiner, Nucl.Phys. **A422** (1984) 103.
- [18] Nguyen van Giai and H. Sagawa, Phys.Lett **B106** (1981) 379.
- [19] P.-G. Reinhard and H. Flocard, Nucl. Phys. **A584** (1995) 467.
- [20] R. B. Firestone, V. S. Shirley, S. Y. F. Chu, C. M. Baglin and J. Zipkin, *Table of Isotopes, John Wiley and Sons, New York* (1996).
- [21] P. Ring and P. Schuck, The nuclear many-body problem (Springer, New York, 1980), sect. 1.4.
- [22] G. M. Temmer, N. P. Heydenberg, Phys. Rev. **104** (1956) 967.
- [23] C. R. Chinn, J. -F. Burger, D. Gogny and M. S. Weiss, Phys. Rev. **C45** (1994) 1700.
- [24] J. Dechargé and D. Gogny, Phys. Rev. **C21** (1980) 1568.
- [25] S. J. Krieger, P. Bonche, H. Flocard, P. -H. Heenen, and M. S. Weiss, Nucl. Phys. **A572** (1994) 384.
- [26] S.J. Krieger, P. Bonche, H. Flocard, P.-H. Heenen, R. Mehrem and M.S. Weiss, Phys. Rev. **C54** (1996) 2399.
- [27] P. Bonche, S. J. Krieger, P. Quentin, M. S. Weiss, J. Meyer, M. Meyer, N. Redon, H. Flocard and P. -H. Heenen, Nucl. Phys. **A500** (1989) 308.
- [28] K.T.R. Davis, H.Flocard, S.J. Krieger and M.S. Weiss, Nucl. Phys. **A342** (1980) 111.
- [29] S.G. Nilsson, C.F. Tsang, A. Sobiczewski, Z. Szymański, S. Wycech, C. Gustafson, I. Lamm, P. Möller and B. Nilsson, Nucl.Phys. **A131** (1969) 1.
- [30] Y.R. Shimizu, private communication.
- [31] T. Bengtsson and I. Ragnarsson, Nucl. Phys. **A436** (1985) 14.

- [32] W.D. Myers and W.J. Swiatecki, *Ark. Phys.* **36** (1967) 343.
- [33] T. Bengtsson, I. Ragnarsson and S. Åberg, in “Computational Nuclear Physics 1”, ed. K. Langanke, J.A. Maruhn and S.E. Koonin, (Springer-Verlag, Berlin, 1991) 51.

FIGURE CAPTIONS

Fig. 1. Potential energy curves of ^{194}Hg for nine parameter sets of the Skyrme force. The abscissa represents the axially symmetric quadrupole deformation parameter δ while the ordinate denotes the energy measured from the sphericity. In parentheses are the excitation energies (in MeV) of the superdeformed minima measured from the ground-state minima at $\delta \sim -0.1$.

Fig. 2. Proton (top) and neutron (middle) pairing gaps and the potential energy curve (bottom) of ^{194}Hg versus the deformation parameter δ calculated with the SkM* force and two sets of pairing force strengths. The solid (dash) curves are calculated with our (Krieger's) strengths. We determine the strengths such that the empirical formula $\bar{\Delta} = 12A^{-1/2}$ MeV is satisfied for Thomas-Fermi level density.

Fig. 3. Neutron(left) and proton(right) single-particle energies versus quadrupole deformation parameter δ for ^{194}Hg obtained by the HF+BCS using SkM*. Positive-parity states are drawn by solid lines and negative-parity states by dashed lines.

Fig. 4. Potential energy curves of ^{236}U versus the deformation parameter δ calculated with the SkM*, SIII, and SkP forces. The ordinate denotes the energy measured from the normal-deformation minimum. The experimental point is also shown with a horizontal error bar.

Fig. 5. Same as in Fig. 4 but for ^{238}U .

Fig. 6. Properties of the superdeformed (i.e., $\delta > 0.35$) minima calculated with the HF+BCS using SkM* force. The top portion displays the quadrupole deformation parameter δ . Nuclei having SD minima are designated with circles whose diameter is proportional to δ of the SD state. Open (solid) circles are used when the SD state is the ground state (an excited state). In the middle portion, the diameter of the circles is inversely

proportional to the excitation energy of the SD minimum. In the bottom portion, the diameter is proportional to the well depth of the SD minimum. Except in the top portion, a circle is not drawn when the SD minimum is the ground state. The grid indices the locations of the magic numbers for spherical shape. The solid staircase-like lines represent the two-proton and the two-neutron drip lines taken from Ref. [6]. Our calculations have been done only for the nuclei between the two-proton drip line and the dashed staircase-like line.

Fig. 7. Potential energy curves of Pb isotopes versus the deformation parameter δ . The ordinate denotes the energy measured from the sphericity. The left, the middle, and the right portions include the curves for $N=94-102$, $N=104-124$, and $N=126-134$, respectively.

Fig. 8. Proton (top) and neutron (middle) pairing gaps and the potential energy curve (bottom) of ^{152}Gd versus the deformation parameter δ calculated with the SkM* force.

Fig. 9. Comparison of the excitation energy E^* of the zero-spin SD states between Krieger's and our results for $Z = 76 - 82$ even-even isotope chains.

Fig. 10. Same as in Fig. 9 but for the barrier heights between the SD and ND wells.

Fig. 11. Same as in Fig. 6 but with the Nilsson-Strutinsky method.

TABLES

Table 1: Comparison of the excitation energy of the SD state at zero-spin in ^{194}Hg between the (extrapolated) experimental value and the predictions of earlier theoretical works.

	E^* (MeV)
experiment[9]	6.017
Woods-Saxon-Strutinsky[10]	4.6
Woods-Saxon-Strutinsky[11, 9]	4.9
HF+BCS with SkM*[8]	5.0
HFB with Gogny D1 [12]	6.9
Nilsson-Strutinsky [13]	7.5

Table 2: Excitation energies E^* and half-lives $\tau_{1/2}$ of the fission isomers in $^{236,238}\text{U}$. The experimental values are compared with the theoretical results by Chinn et al. and Krieger et al. as well as with our results using the SkM* force. As for the half-lives, our calculation depends on the enhancement factor for the collective mass f_B .

	E^* (MeV)		$\tau_{1/2}$ (sec)	
	^{236}U	^{238}U	^{236}U	^{238}U
experiment [20]	2.750	2.557	1.20×10^{-7}	2.98×10^{-7}
Chinn et al. [23]	—	2.828	—	8.5×10^{-5}
Krieger et al. [25] w/o GCM	—	3.0	—	—
Krieger et al. [25] with GCM	—	2.28	—	$0.05\text{-}20 \times 10^{-9}$
Krieger et al. [26] w/o GCM	2.9	2.7	—	—
Krieger et al. [26] with GCM	2.77	2.61	3.7×10^{-8}	8.5×10^{-9}
ours with $f_B=10$	4.5	3.3	1.3×10^{-9}	1.6×10^{-7}
ours with $f_B=20$	4.5	3.3	8.4×10^{-5}	7.8×10^{-2}
ours with $f_B=30$	4.5	3.3	4.1×10^{-1}	1.8×10^3
ours with $f_B=40$	4.5	3.3	5.3×10^2	8.4×10^6

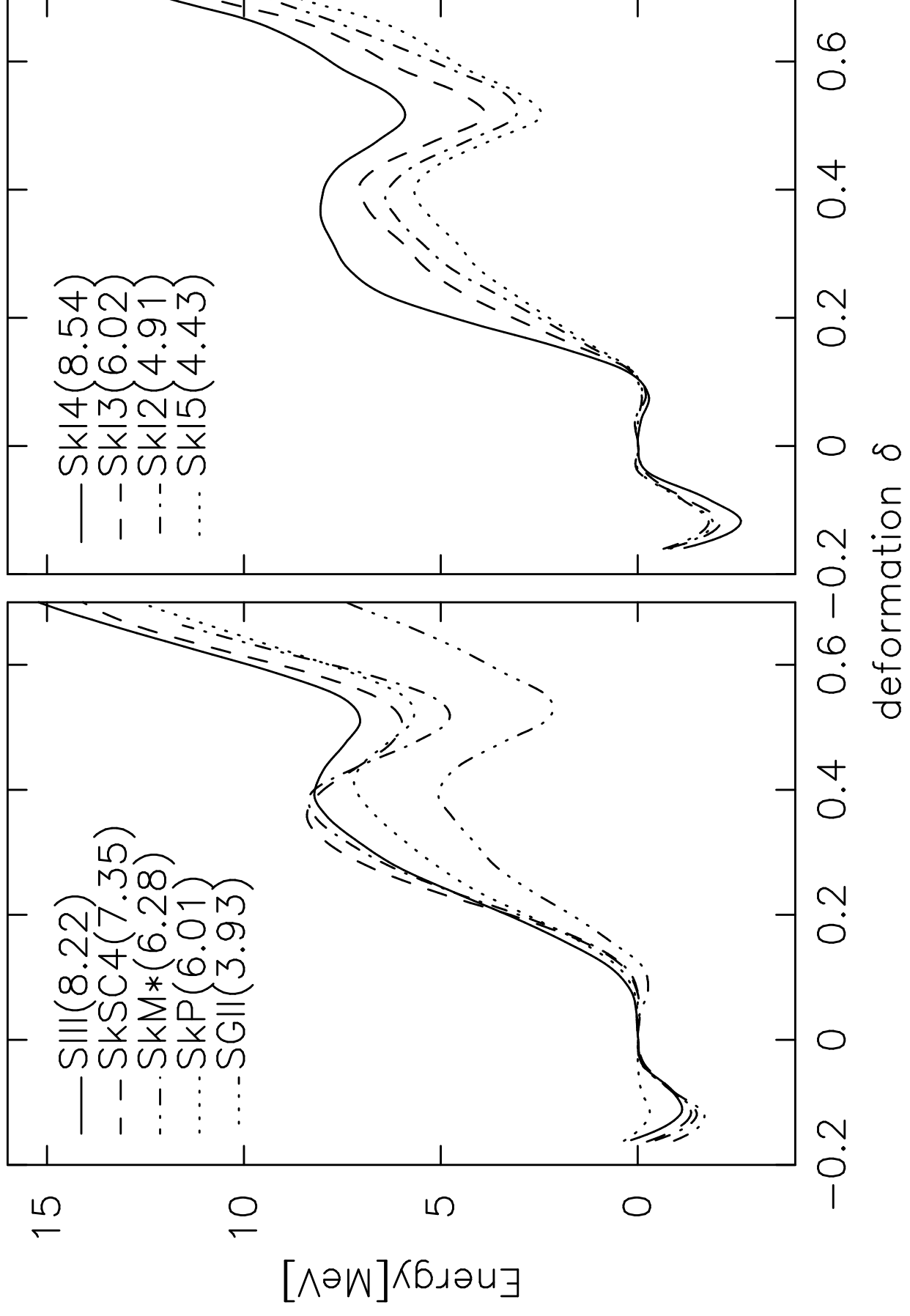
Table 3: Properties of SD minima in $20 \leq Z \leq 82$ even-even nuclei calculated with the HF+BCS method using the SkM* force and a seniority pairing force. The columns present the atomic number Z , the neutron number N , the deformation δ , the excitation energy E^* , and the barrier height E_B . A letter “g” in the first column indicates that the SD minimum is the ground state, while a character “*” means that it is an excited state having a rather low excitation energy (< 8 MeV) and not a too shallow barrier height (> 0.5 MeV).

Table 3:

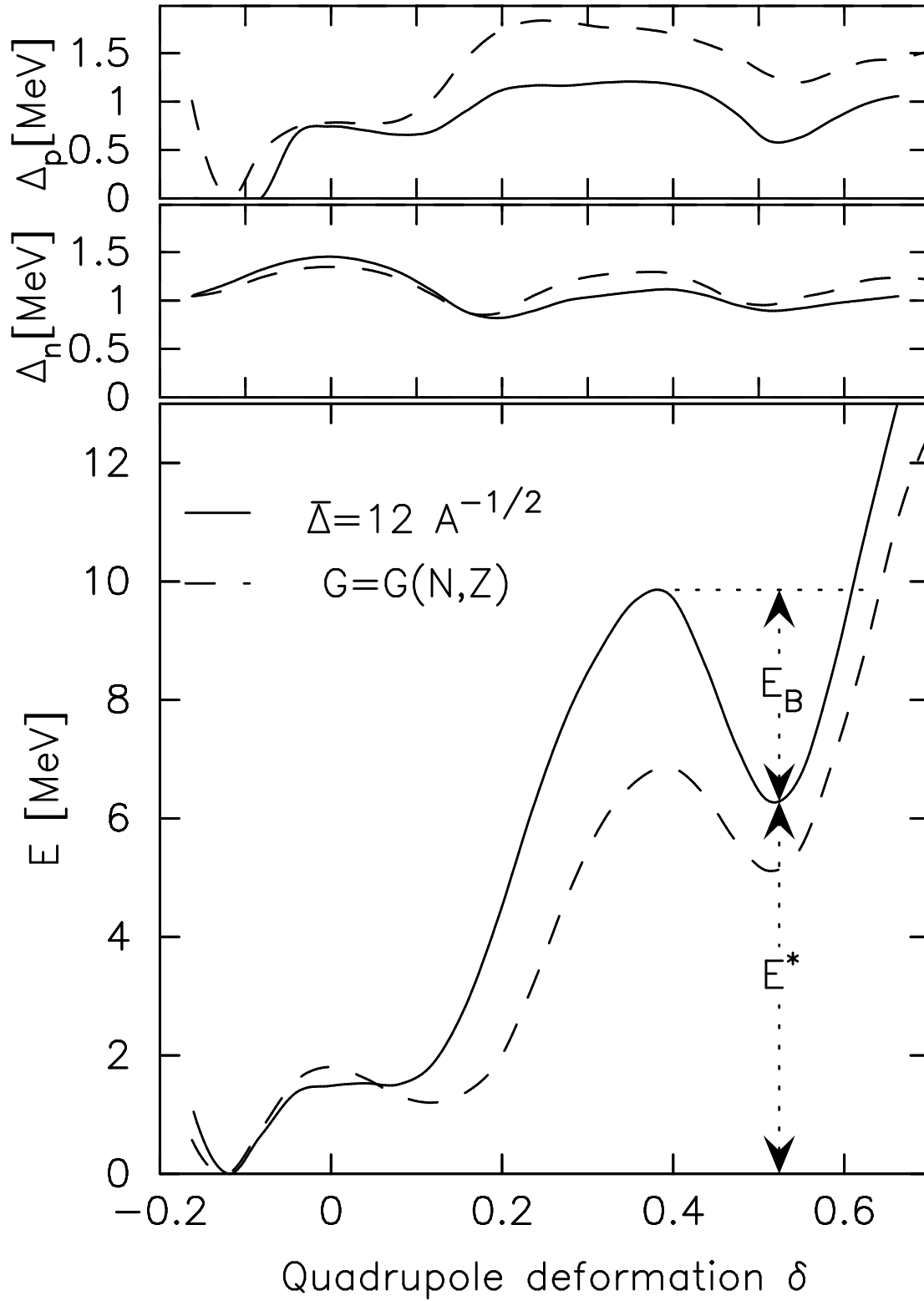
	Z	N	δ	E^* (MeV)	E_B (MeV)		Z	N	δ	E^* (MeV)	E_B (MeV)
σ	36	36	0.38				48	80	0.56	21.80	0.13
σ	36	38	0.38				50	80	0.56	25.67	0.05
σ	36	40	0.36			g	58	60	0.35		
	38	34	0.36	0.23	0.11	g	58	62	0.36		
σ	38	36	0.39			g	58	64	0.36		
σ	38	38	0.40				58	80	0.44	9.31	0.12
σ	38	40	0.39			g	60	62	0.37		
σ	38	42	0.36			g	60	64	0.36		
σ	38	60	0.36			g	60	66	0.35		
σ	38	62	0.37				64	90	0.61	8.02	0.08
σ	38	64	0.37				64	92	0.60	9.53	0.07
σ	38	66	0.36				68	80	0.51	6.37	0.00
σ	40	38	0.40				68	84	0.43	7.13	0.01
σ	40	40	0.41				70	80	0.53	6.91	0.02
σ	40	62	0.36				70	82	0.43	10.86	0.01
σ	40	64	0.37				70	84	0.43	7.63	0.12
σ	40	66	0.36				72	80	0.53	7.56	0.23
σ	40	68	0.35				72	82	0.43	11.75	0.66
σ	42	38	0.38				72	84	0.43	8.47	0.78
σ	42	40	0.37				72	86	0.41	5.93	0.35
*	44	44	0.62	6.69	0.53		74	84	0.50	9.96	2.20
	44	46	0.62	9.91	0.51		* 74	86	0.48	7.35	1.44
	44	48	0.61	13.73	0.23		74	88	0.46	5.84	0.39
	44	50	0.65	16.28	0.33		74	114	0.47	6.25	0.13
	46	44	0.63	8.83	0.86		74	116	0.48	6.66	0.36
	46	46	0.68	11.88	1.04		74	118	0.46	6.14	0.19
	46	48	0.64	16.29	0.33		76	86	0.52	8.65	3.27
	48	44	0.63	11.70	0.74		* 76	88	0.51	6.76	1.80
	48	46	0.66	15.14	0.64		76	90	0.47	5.78	0.46
	48	48	0.62	19.62	0.07		76	110	0.47	5.50	0.12

Table 3 - continued

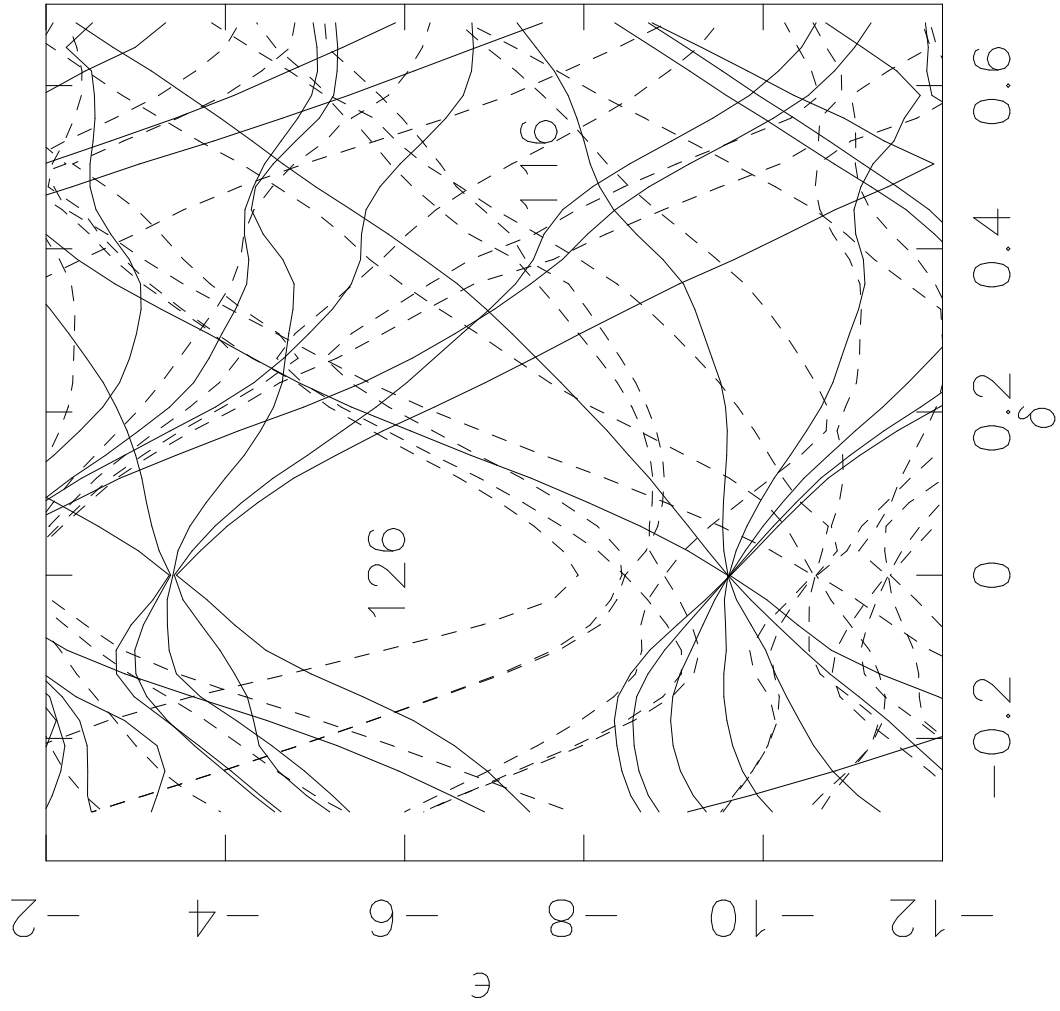
	Z	N	δ	E^* (MeV)	E_B (MeV)		Z	N	δ	E^* (MeV)	E_B (MeV)
*	76	112	0.49	5.93	0.67	*	80	116	0.52	7.36	5.41
*	76	114	0.49	6.47	1.30	*	80	118	0.52	7.60	5.82
*	76	116	0.49	7.18	1.80		80	120	0.52	11.79	5.73
*	76	118	0.50	7.23	1.88		80	122	0.51	14.13	5.79
	76	120	0.48	8.23	1.89		80	124	0.51	16.94	5.89
	76	122	0.47	10.19	2.16		80	126	0.50	19.90	6.14
*	78	88	0.55	7.70	3.80		80	128	0.51	16.75	6.00
*	78	90	0.55	5.95	2.21		80	130	0.51	13.70	6.06
*	78	92	0.54	5.08	0.86	*	82	94	0.59	6.13	2.73
	78	94	0.52	4.57	0.10	*	82	96	0.59	5.28	1.97
	78	108	0.47	3.47	0.10	*	82	98	0.60	4.72	1.18
*	78	110	0.49	3.76	0.75		82	100	0.62	4.14	0.42
*	78	112	0.51	4.21	1.55		82	102	0.63	3.78	0.27
*	78	114	0.51	4.85	2.32		82	106	0.55	3.84	0.05
*	78	116	0.51	5.89	3.60	*	82	108	0.55	4.10	0.94
*	78	118	0.51	7.06	3.88	*	82	110	0.55	4.65	2.36
	78	120	0.50	9.21	3.77	*	82	112	0.54	5.58	3.76
	78	122	0.49	12.13	3.79	*	82	114	0.54	6.86	4.79
	78	124	0.49	15.07	4.10		82	116	0.54	8.55	5.59
	78	126	0.48	18.07	4.42		82	118	0.54	10.75	6.20
*	80	92	0.56	5.20	2.91		82	120	0.53	13.84	6.14
*	80	94	0.56	4.51	1.96		82	122	0.52	17.11	6.06
*	80	96	0.55	4.12	1.20		82	124	0.50	20.17	6.32
	80	98	0.53	3.96	0.48		82	126	0.50	23.05	6.51
	80	100	0.48	3.60	0.06		82	128	0.49	19.75	6.39
	80	106	0.50	3.45	0.14		82	130	0.50	16.69	6.28
*	80	108	0.52	3.69	1.06		82	132	0.51	13.72	6.28
*	80	110	0.52	4.12	2.38		82	134	0.52	10.85	6.34
*	80	112	0.52	4.86	3.62						
*	80	114	0.52	6.27	3.59						



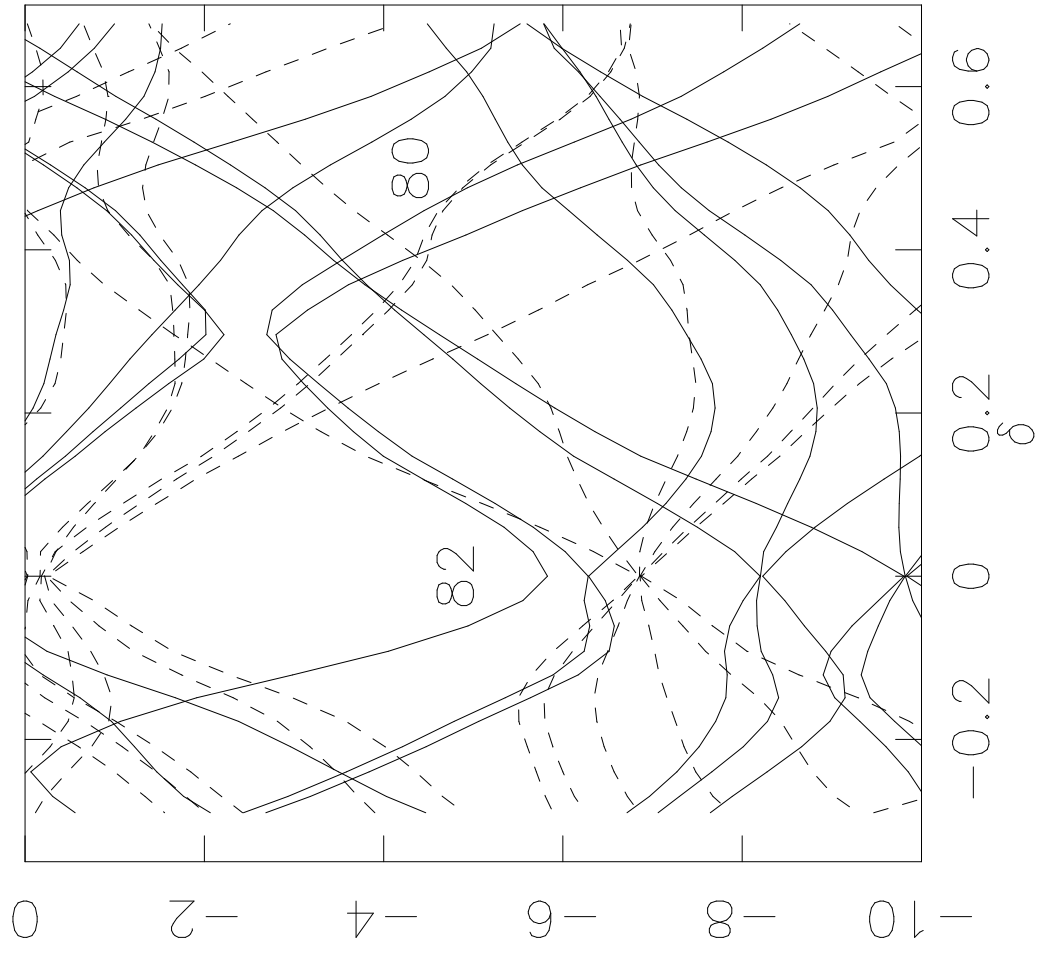
^{194}Hg SkM*

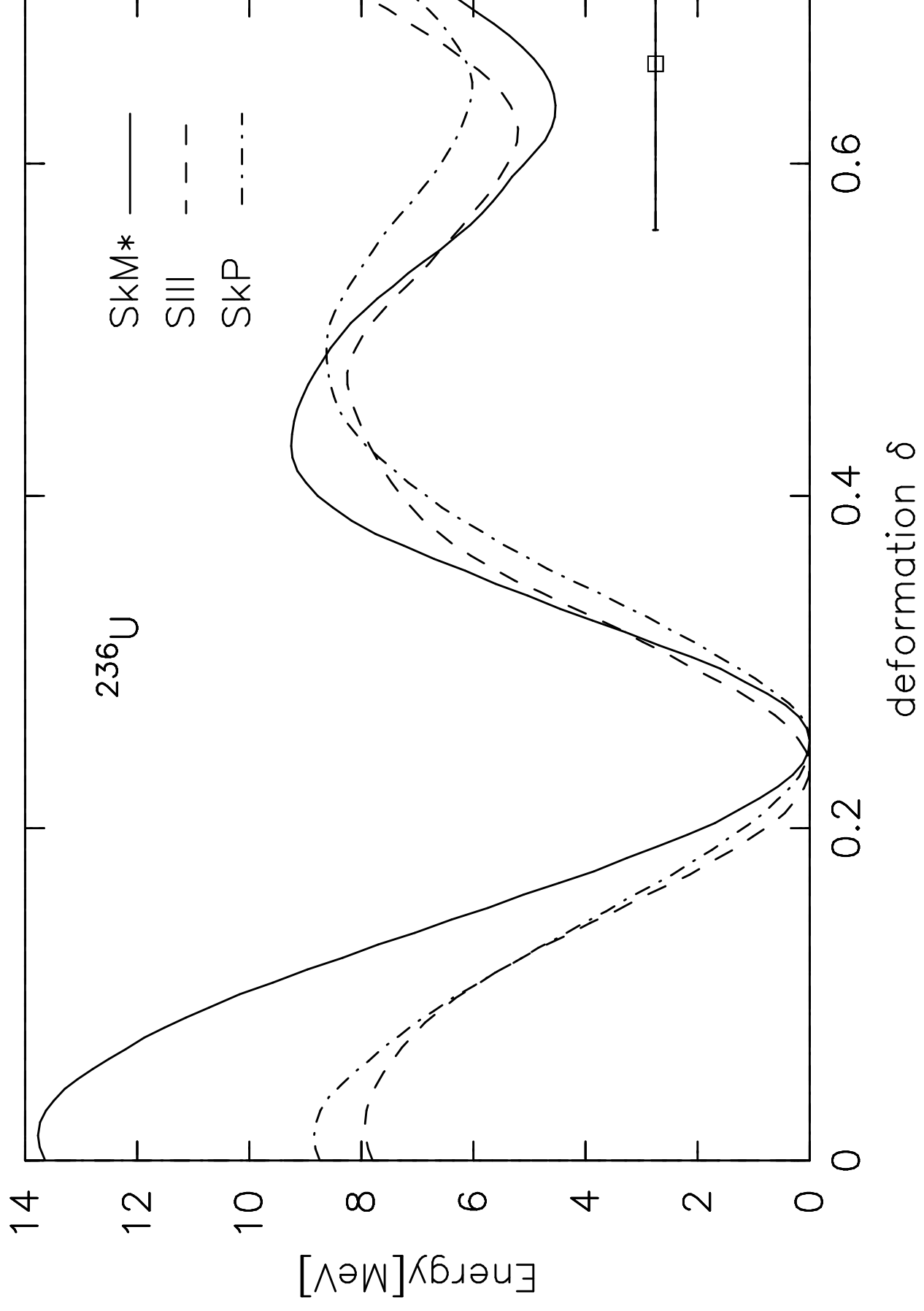


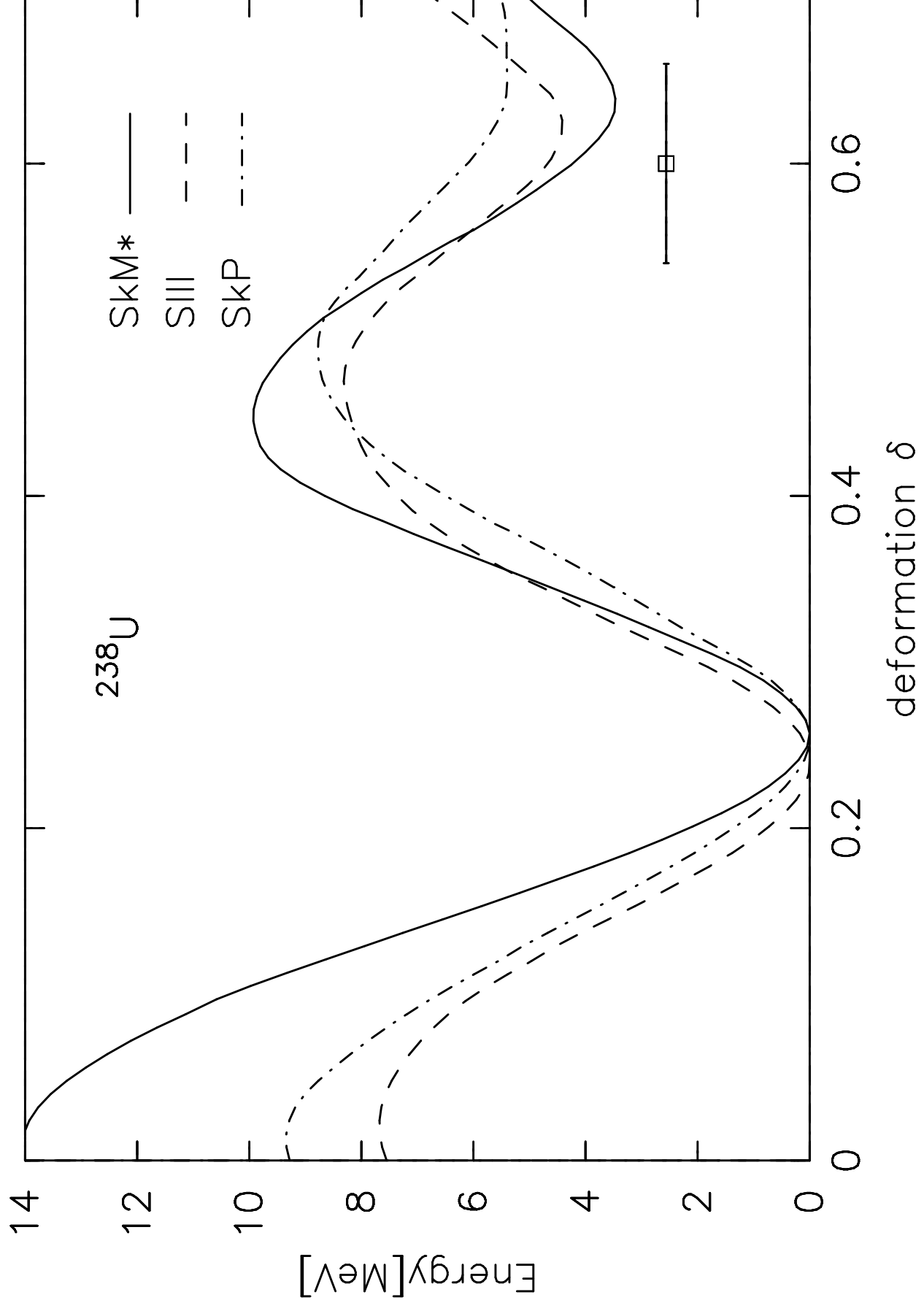
Neutron

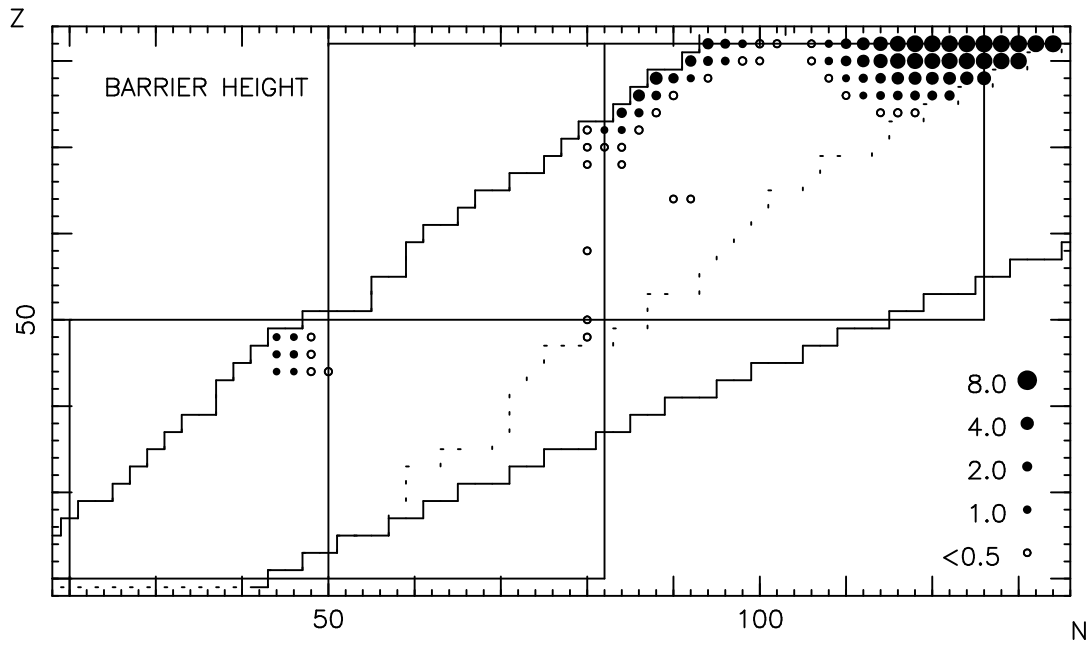
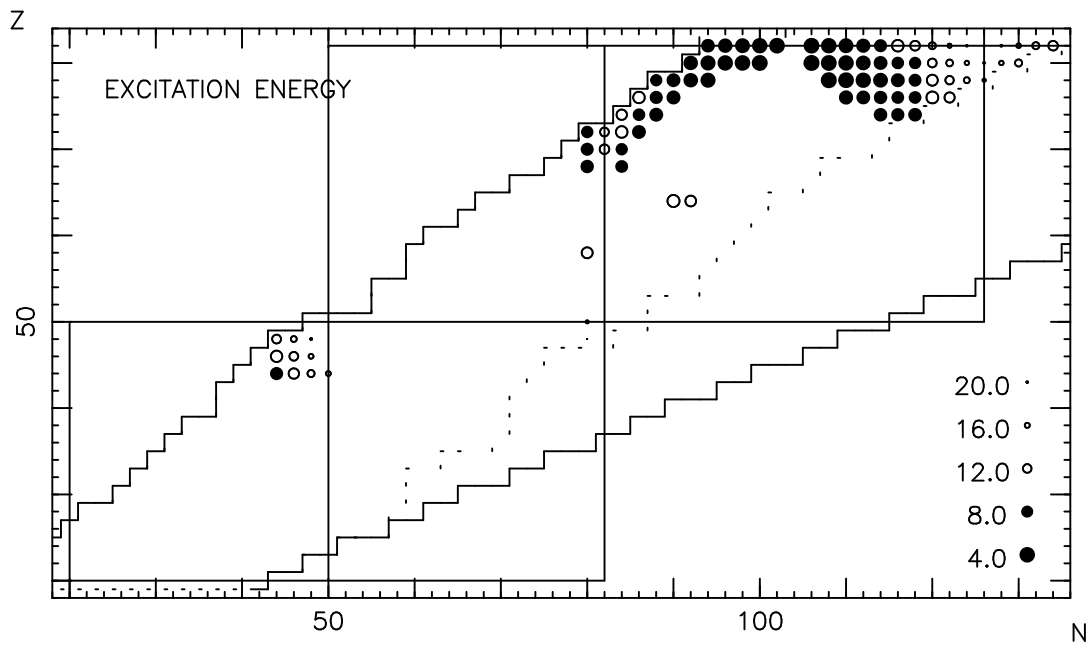
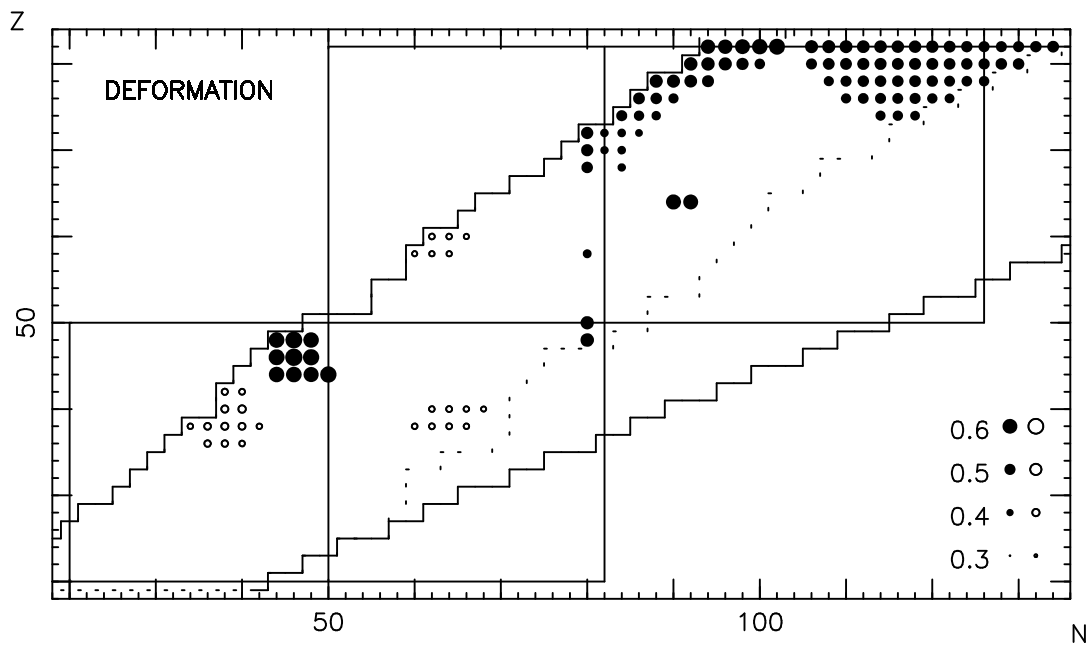


Proton

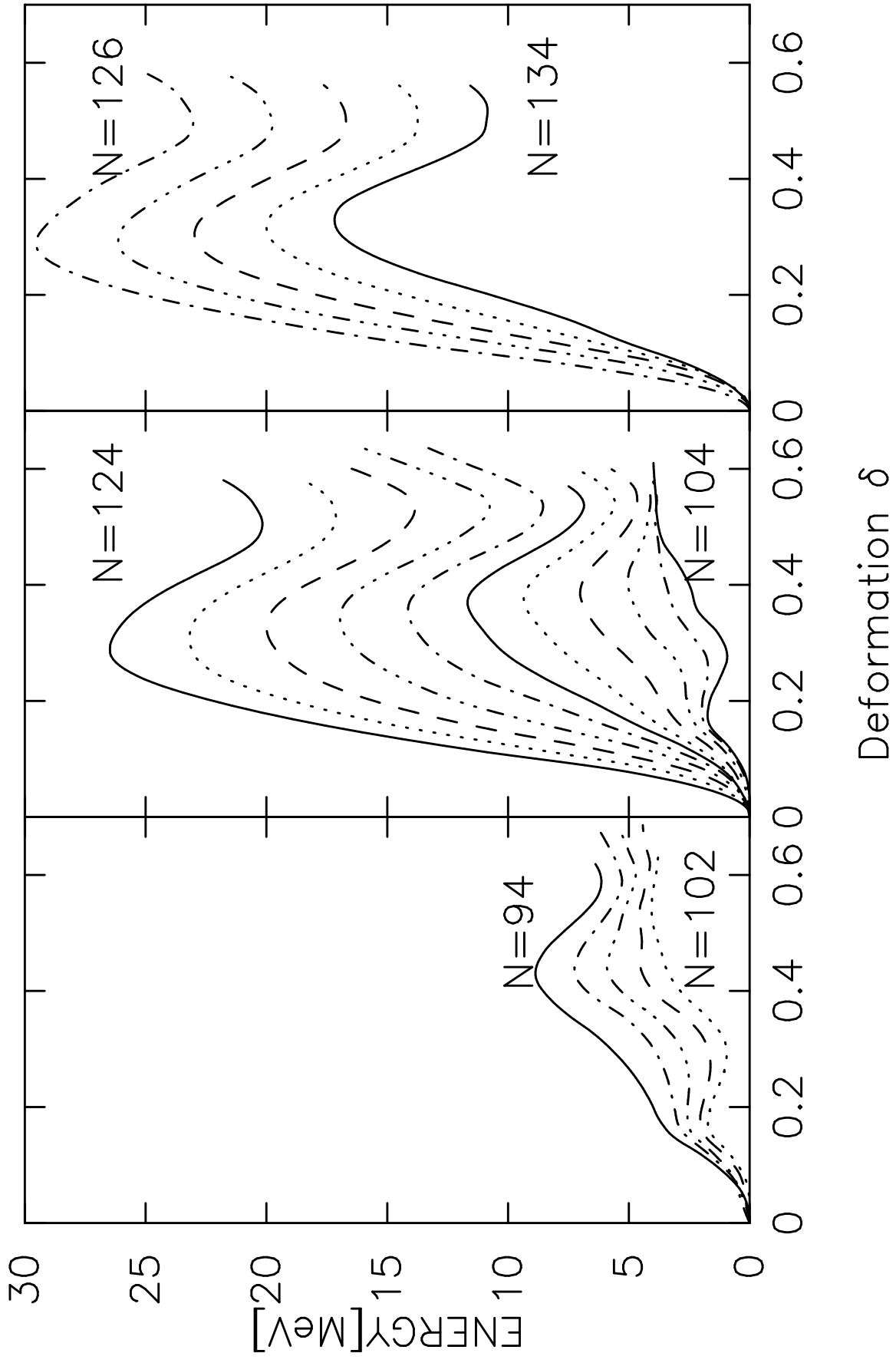








Pb SkM*



^{152}Gd SkM*

